

## Local vibrational modes of Ge-rich $c\text{-Si}_{1-x}\text{Ge}_x$ alloys

C. H. Grein\* and M. Cardona

*Max-Planck-Institut für Festkörperforschung, Heisenbergstrasse 1, D-7000 Stuttgart 80, Federal Republic of Germany*

(Received 12 July 1991; revised manuscript received 7 November 1991)

The local vibrational modes of Ge-rich  $c\text{-Si}_{1-x}\text{Ge}_x$  alloys ( $x \geq 0.75$ ) are calculated using a parameter-free, mass-defect Green's-function approach. A microscopic expression of the Raman-scattering efficiency is then evaluated for inelastic light scattering from these modes. Particular attention is paid to the modes which are responsible for the fine structure in the phonon spectra which is observed in addition to the strong Ge-Ge, Si-Si, and Si-Ge modes. The corrections to the extended Ge-Ge modes due to alloy disorder are calculated with use of the coherent-potential approximation and also included in the Raman susceptibility.

### I. INTRODUCTION

The elastic and vibrational properties of semiconductor alloys have recently received renewed attention, particularly those of the technologically important  $\text{Si}_{1-x}\text{Ge}$  alloys and Si/Ge superlattices. A continuing problem with these materials is the 4% lattice mismatch between bulk Si and Ge, which leads to misfit dislocations or strained layers in Si/Ge superlattices.<sup>1,2</sup> Related effects, such as strain-induced ordering in molecular-beam-epitaxy-(MBE) grown  $\text{Si}_{1-x}\text{Ge}_x$  alloy films and layers, have been studied in Refs. 3–5; Monte Carlo simulations suggest that such ordering is not a bulk effect.<sup>6</sup> Certain strain relaxation mechanisms have recently been reported in Ref. 7.

Questions such as the presence of ordering may be examined by studying the phonon spectra of the alloys. The vibrational properties are also of interest due to the multiple-mode behavior observed in the phonon spectra of some of these materials.<sup>8</sup> Infrared absorption and Raman-scattering studies of the vibrational modes of  $c\text{-Si}_{1-x}\text{Ge}_x$  alloys include Refs. 9–15. Many of these measurements show the existence of considerable fine structure in the phonon spectra in addition to the stronger Ge-Ge ( $\sim 300\text{ cm}^{-1}$ ), Si-Ge ( $\sim 400\text{ cm}^{-1}$ ), Si-Si ( $\sim 500\text{ cm}^{-1}$ ) modes<sup>13</sup> which are observed for most choices of  $x$  from the pure Ge and pure Si limits. A fundamental question concerning the fine structure is the microscopic origin of these vibrational modes. They have been interpreted as signatures of long-range order,<sup>16</sup> or as intrinsic features of disorder.<sup>11,14</sup> A fit to the composition dependence of the Si-Si, Ge-Ge, and Si-Ge mode frequencies has been made by Zinger *et al.*<sup>17</sup> using a random element isodisplacement model (REIM);<sup>18</sup> however, this model does not provide a correct microscopic picture since all modes are assumed to be extended, yet some modes in Ge-rich  $c\text{-Si}_{1-x}\text{Ge}_x$  are localized.<sup>19</sup> Moreover the REIM is ill-suited to describe the detailed fine structure that is seen experimentally. A recent model of the vibrational properties of  $c\text{-Si}_{1-x}\text{Ge}_x$  (Ref. 14) avoids the REIM by considering supercells with lattice sites randomly occupied by Si and Ge atoms and calculates the phonon modes using a Keating potential.<sup>20</sup> Unfortunately this

model was insufficiently precise to identify many of the modes between 400 and 480  $\text{cm}^{-1}$  responsible for the fine structure in the Raman spectra of Ge-rich  $c\text{-Si}_{1-x}\text{Ge}_x$ . This may be a consequence of deficiencies in the Keating-model dynamics or possibly statistical effects due to the supercell approach.

To conclusively identify the vibrational modes responsible for the fine structure observed in the Raman spectra of Ge-rich  $c\text{-Si}_{1-x}\text{Ge}_x$  we use a parameter-free cluster approach. As described in Sec. II, a mass-defect Green's-function method is employed to obtain the frequencies and modes of local phonons due to the most probable cluster of Si atoms that occur in the Ge-rich material. We then calculate the Raman-scattering efficiency due to inelastic light scattering from these local modes, together with scattering from the extended Ge-Ge mode. In Sec. III, a comparison with experimental data is made, and results are summarized in Sec. IV.

### II. CALCULATION OF THE LOCAL VIBRATIONAL MODES AND THE RAMAN SPECTRA

The disorder present in semiconductor alloys leads to the possibility of localized electronic and vibrational states. Since localized states are nonperturbative with respect to extended states, it is not possible to employ any computational scheme based on perturbation theory to describe such states. In this section, a nonperturbative approach to calculate the localized vibrational states of semiconductor alloys is presented. Also, the expressions for the Raman-scattering efficiency for inelastic light scattering from such localized vibrational modes are obtained.

To calculate the local phonon modes of Ge-rich  $c\text{-Si}_{1-x}\text{Ge}_x$  we employ a mass-defect Green's-function approach. After the pioneering work of Lifshitz,<sup>21</sup> the earliest works employing such an approach include the study of the local vibrations of single isolated mass defects by Dawber and Elliott,<sup>19</sup> and defect pairs in silicon by Elliott and Pfeuty.<sup>22</sup> Here, we extend these methods to model  $c\text{-Si}_{1-x}\text{Ge}_x$  with somewhat higher concentrations of Si atoms ( $1-x$  as much as  $\sim 0.25$ ) than previous calculations of this type have been able to consider.

The model we employ for  $c\text{-Si}_{1-x}\text{Ge}_x$  is that of isolated clusters of Si atoms embedded in the virtual crystal. In the results to be described, all 32 possible clusters of a single atom and its four nearest neighbors (with each of the five atoms being either a Si or a Ge atom) are considered. For Ge-rich alloys, the larger the number of Si atoms in a cluster the more improbable this type of cluster is. To approximate the effects of a distribution of Si and Ge atoms outside of the clusters, the latter are assumed to be embedded in the virtual crystal of the alloy rather than in pure Ge. To obtain the total vibrational spectra the contributions of different clusters are weighted by their probabilities of occurrence, assuming a completely random mixture. This model describes, in an approximate fashion, the possible configurations of Ge-rich alloys (it could also be used to model Si-rich materials), becoming better the lower the concentration of Si atoms.

The general equations for the local vibrational frequencies and normal modes of mass defects in otherwise perfect crystals may be derived from the relevant equation of motion.<sup>19</sup> To indicate how these equations are employed in our cluster approach we present some of the main results of Ref. 19 and describe our modifications. The vibrational modes of a lattice with substitutional defects may be described by the displacements.

$$u_\alpha(l) = \sum_f \chi_\alpha(f, l) \left[ \frac{\hbar}{2\omega_f} \right]^{1/2} [a^\dagger(f) + a(f)], \quad (2.1)$$

where  $f$  labels the modes of frequency  $\omega_f$  in an  $N$ -unit-cell crystal with masses  $M_\alpha(l)$  in unit cell  $l$  at position  $\mathbf{R}_l$ , the lower case greek letters denote the six Cartesian components of the two atoms per unit cell,  $a(f)$  is the destruction operator for mode  $f$ , and the  $\chi_\alpha(f, l)$  are obtained by solving the equation of motion

$$\chi_\alpha(f, l) = \sum_{\beta, l'} \sum_{\gamma, l''} G_{\alpha\beta}(l, l'', \omega) C_{\beta\gamma}(l'', l') \chi_\gamma(f, l'). \quad (2.2)$$

Here,  $G$  is the virtual-crystal-phonon Green's function

$$G_{\alpha\beta}(l, l', \omega) = \frac{1}{NM_{\text{VCA}}} \sum_{\mathbf{k}, j} \frac{\sigma_\alpha^{*j}(\mathbf{k}) \sigma_\beta^j(\mathbf{k}) e^{-i\mathbf{k} \cdot (\mathbf{R}_l - \mathbf{R}_{l'})}}{\omega_j^2(\mathbf{k}) - \omega^2}, \quad (2.3)$$

where  $(j, \mathbf{k})$  label the mode branch and wave vector of the virtual-crystal phonons of frequency  $\omega_j(\mathbf{k})$  with  $M_{\text{VCA}} = (1-x)M_{\text{Si}} + xM_{\text{Ge}}$  being the virtual-crystal atomic mass, and the  $\sigma_\alpha^j(\mathbf{k})$  are the polarization vectors. In the approach described in Refs. 19 and 22 the Green's function was that of the pure host material rather than the virtual crystal. The latter eliminates trivial first-order perturbation corrections. The defects are described by the matrix

$$C_{\alpha\beta}(l, l') = [M_{\text{VCA}} - M_\alpha(l)] \omega^2 \delta_{\alpha\beta} \delta_{ll'} + \Delta A_{\alpha\beta}(l, l'), \quad (2.4)$$

where the first term represents the mass defects and the second force-constant changes. In Ge-rich  $c\text{-Si}_{1-x}\text{Ge}_x$  the ratio of the defect (Si) to host (Ge) masses is 0.387, whereas the corresponding force-constant ratio in a Keat-

ing model<sup>20</sup> is  $\alpha_{\text{Si-Si}}/\alpha_{\text{Ge-Ge}} = 1.13$ .<sup>14</sup> Thus the mass-defect contributions are expected to dominate and the second term in (2.4) may be neglected. The normalization condition for the  $\chi_\alpha$  is taken to be

$$\sum_{\alpha, l} M_\alpha(l) |\chi_\alpha(f, l)|^2 = 1. \quad (2.5)$$

The above expressions are valid for both local and resonant modes. However, for resonant modes, the Green's function (2.3) has poles on the real axis and (2.2) becomes an  $6N \times 6N$  set of equations for  $\chi_\alpha$ . As a consequence, the numerical study of resonant modes is considerably more difficult than that of local modes. Thus we concentrate on local modes in this study. However, it is difficult to decide *a priori* which modes are resonant and which are local. If the mobility edge (that is, the energy boundary between local and extended modes) moves linearly with the alloy composition ratio, as it does in the virtual-crystal approximation, one would expect that Raman-active modes above  $400 \text{ cm}^{-1}$  will remain local for Si concentrations up to  $1-x \sim 0.5$ . Thus it may be assumed that for any reasonably smooth behavior of the mobility edge the Raman-active modes will all be local up to  $1-x \sim 0.25$ , which is therefore the most Si-rich alloy we study.

The vibrational frequencies and normal modes are obtained by solving the eigenvalue equation (2.2). For local modes in Ge-rich  $c\text{-Si}_{1-x}\text{Ge}_x$  a further simplification is possible due to the large mass difference between the defect and virtual-crystal atoms. This involves solving (2.2) and (2.5) only for those  $l$  which are defect atoms in the clusters under consideration, thus neglecting the small vibrational amplitudes of the more massive Ge atoms in modes which are strongly localized on defect sites. Then (2.2) is a  $15 \times 15$  equation for the largest (five-atom) clusters we consider.

The computational procedure that was employed was to evaluate the virtual-crystal Green's function (2.3) with phonon frequencies and polarization vectors obtained from an adiabatic bond charge model<sup>23</sup> at 2361 points in the entire Brillouin zone. The bond charge model is among the best methods for computing the phonon spectra and normal modes of ordered diamond-structure semiconductors.<sup>24</sup> The vibrational frequencies and normal modes of the local vibrations of the 32 five-atom clusters (calculations are simplified when one notes that many of the configurations are equivalent to one another) were then obtained by solving for the eigenfrequencies and eigenvectors of (2.2) for each cluster configuration. As a check on the validity of neglecting the force-constant changes in (2.4), the frequencies of the clusters with exactly two adjacent Si atoms were computed both with and without nearest-neighbor force-constant changes as given by the Keating parameters used in Ref. 14. The differences were found to be approximately 1%.

The results of the computations are a large number of modes, those involving clusters containing three or more Si atoms typically being rather complicated and asymmetric. To test the validity of our results we have calculated the first-order Raman spectra of the local modes. This selects the most Raman-active modes from all those

that were calculated and thus makes comparison with experiment easier. The calculation was done employing the microscopic method of Ref. 25 by summing over the dominant 12 Feynman diagrams (six for the electron emitting a phonon, and six for the hole) which contribute to off-resonance first-order Stokes Raman scattering to obtain the scattering efficiency. These diagrams are shown in Figs. 1(a) and 1(b). The diagrams are isomorphic to those discussed in Ref. 25 except that phonon crystal momentum is no longer a quantum number for local modes, only energy can be used to label these states. The electronic structure is calculated using local empirical pseudopotentials in the virtual-crystal approximation, that is, contributing electronic states are assumed to be well away from mobility edges on the extended-state side. In these cases, the effect of disorder on the electronic structure is known to be small.<sup>26</sup> We note that the usual phonon  $q=0$  crystal momentum selection rule of first-order Raman scattering in ordered crystals holds only approximately for scattering from local modes. The local phonon can scatter the electron from any state to any other, but overall crystal momentum conservation requires less probable (due to the low concentration of scattering centers) diagrams of the type shown in Fig. 1(c) to describe those scattering events where the phonon emission does not preserve the electron crystal momentum. Our calculations only include the twelve dominant diagrams Figs. 1(a) and 1(b) which describe zero-momentum transfer during phonon emission.

In terms of the plane-wave expansion of the Bloch function

$$|n\mathbf{k}\rangle = \frac{1}{\sqrt{V}} \sum_{\mathbf{G}} c_{n\mathbf{k}}(\mathbf{G}) \exp[i(\mathbf{k} + \mathbf{G}) \cdot \mathbf{r}], \quad (2.6)$$

$$\langle n\mathbf{k} | H_{e-ph} | n'\mathbf{k}' \rangle_f = \frac{i}{2N} \left( \frac{\hbar}{2\omega_f} \right)^{1/2} \sum_{l,\alpha} \sum_{\mathbf{G},\mathbf{G}'} c_{n\mathbf{k}}^*(\mathbf{G}) (\mathbf{k} - \mathbf{k}' + \mathbf{G} - \mathbf{G}')_{\alpha} \tilde{V}_{VC}(\mathbf{k} - \mathbf{k}' + \mathbf{G} - \mathbf{G}') c_{n'\mathbf{k}'}(\mathbf{G}') \times e^{-i(\mathbf{k} - \mathbf{k}' + \mathbf{G} - \mathbf{G}') \cdot (\mathbf{R}_l + \boldsymbol{\tau})} \chi_{\alpha}(f, l), \quad (2.7)$$

where  $\boldsymbol{\tau}$  gives the positions of the two atoms in the unit cell in a bond-centered coordinate system [ $\boldsymbol{\tau} = a(1, 1, 1)/8$  if  $\alpha \leq 3$ ,  $\boldsymbol{\tau} = -a(1, 1, 1)/8$  if  $\alpha \geq 4$ ;  $a$  being the lattice spacing], and  $\tilde{V}_{VC}$  are the virtual-crystal pseudopotentials, obtained from Cohen and Bergstresser.<sup>27</sup> Since the index  $\alpha$  may run from 1 to 6, the wave vectors and reciprocal-lattice vectors in the term  $(\mathbf{k} - \mathbf{k}' + \mathbf{G} - \mathbf{G}')_{\alpha}$  may be taken to be six component vectors with the first three components equal to the last three.

In the notation of Ref. 25, the scattering efficiency is given by

$$\frac{\partial^2 S}{\partial \Omega \partial \omega_R} = \left( \frac{\omega_s}{c} \right)^4 \sum_{\alpha, \beta, \gamma, \delta=1}^3 I_{\alpha\beta\gamma\delta} \hat{e}_L \hat{e}_{L\alpha}^* \hat{e}_S \hat{e}_{S\beta}^* \hat{s}_{\delta}, \quad (2.8)$$

where, in terms of the Raman tensor  $a_{\alpha\beta}$ ,  $I_{\alpha\beta\gamma\delta}$  is

$$I_{\alpha\beta\gamma\delta} = \frac{1}{N} \sum_f a_{\alpha\beta}(f) a_{\gamma\delta}(f) \delta(\omega_R - \omega_f) [n(\omega_f) + 1], \quad (2.9)$$

and

$$a_{\alpha\beta}(f) = \frac{1}{N} \sum_{\mathbf{k}, c, c', v, v'} [\chi'_{\alpha\beta}(\mathbf{k}v v' c c') (\delta_{cc'} \langle v\mathbf{k} | H_{e-ph} | v'\mathbf{k} \rangle_f - \delta_{vv'} \langle c\mathbf{k} | H_{e-ph} | c'\mathbf{k} \rangle_f + \dots)]. \quad (2.10)$$

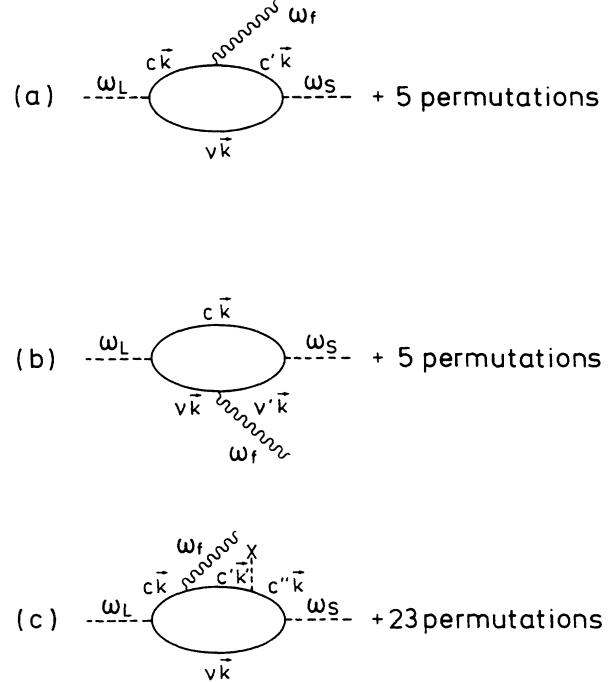


FIG. 1. Feynman diagrams describing first-order Stokes Raman scattering where the electron (a) or the hole (b) emits a local phonon. The diagrams not drawn are obtained by permuting the vertices of the shown diagrams. (c) Shows a less probable (for Ge-rich  $c\text{-Si}_{1-x}\text{Ge}_x$ ) contribution arising from the electron scattering from a Si potential after emitting a phonon.

where  $V$  is the volume of the virtual crystal, the deformation-potential electron local-phonon interaction is

The ellipsis in (2.10) represents the ten other terms obtained by permuting the vertices of the diagrams in Figs. 1(a) and 1(b), the Bose function is  $n(\omega) = [\exp(\hbar\omega/k_B T) - 1]^{-1}$ , and the differential susceptibility  $\chi'$  is defined in Ref. 28. The numerical procedure employed to evaluate the above expressions is detailed in Ref. 25; the wave-vector sum in (2.10) was performed over 89 points in an irreducible  $\frac{1}{48}$  wedge of the Brillouin zone.

The above procedure provides the frequencies and normal modes of the local vibrations associated with a low concentration of Si defects. To treat the extended phonon modes associated with the vibrations seen in pure Ge, we employ the coherent-potential approximation (CPA).<sup>29</sup> Using this method the frequency shifts and broadenings of extended modes due to alloy disorder may be computed using, for example, the pure Ge modes given by the bond charge model as reference spectra. We have employed the CPA and bond charge model to calculate the shifts and broadenings of  $O(\Gamma)$  Ge phonons as a function of Si concentration and have included their contributions to the Raman spectra calculated for the local modes. Further details concerning the application of the CPA method may be found in Ref. 30, and the calculation of the Raman spectra of extended modes in Ref. 25.

### III. DISCUSSION

The calculated frequency of the  $O(\Gamma)$  Ge phonons is shown in Fig. 2 and compared with two sets of experimental data. An interesting feature of the measurements is the strong initial rise in the Ge-Ge frequency with increasing Si content, followed by a roughly linear downward slope. The CPA calculations do not reproduce the initial rise. We have been able to model the observed behavior by performing calculations which include both diagonal (mass defect) and off-diagonal (bond length and

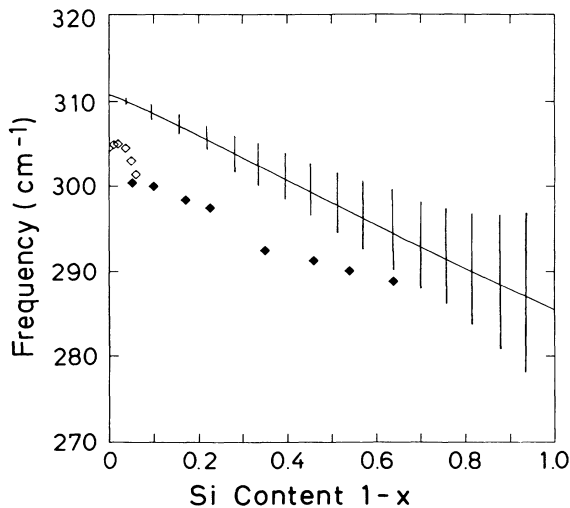


FIG. 2. Frequency of the Ge extended mode as a function of alloy composition calculated with the coherent-potential approximation. The vertical lines indicate the broadening due to alloy scattering. Open symbols are experimental data from Ref. 31, and solid symbols are data from Ref. 13.

angle) disorder. These results are reported elsewhere.<sup>31</sup> Since the CPA method we have employed includes only diagonal disorder, it underestimates the initial rise; however, it does provide a good overall description of the real self-energy shift of the phonon. The  $O(\Gamma)$  frequency for pure Ge is about  $5 \text{ cm}^{-1}$  too high, a deficiency of the bond charge model parameters used. Also shown in Fig. 2 (vertical lines) is the calculated full width at half maximum (FWHM) broadening of the  $O(\Gamma)$  phonons due to alloy disorder. The calculated widths, plus the lifetime broadening due to anharmonic decay, agree well with measurements reported in Ref. 13.

For local modes in the limit of a very low Si concentration, the calculated frequency of vibration of an isolated Si atom in a Ge host is  $378.5 \text{ cm}^{-1}$ . The  $\text{TA}(2\Gamma_3^-)$ ,  $\text{TO}(2\Gamma_3^+)$ , and  $\text{LO}(\Gamma_1^+)$  modes of a pair of adjacent Si atoms in a Ge host have frequencies 371.9, 384.6, and  $435.0 \text{ cm}^{-1}$ , respectively. The LA mode for the defect pair is found to be resonant with the background.

To estimate the degree of localization of the vibration of an isolated Si atom, we have evaluated the participation ratio for this ratio, defined as<sup>32</sup>

$$p^{-1} = \frac{\sum_{j=1}^{2N} (\mathbf{u}_j \cdot \mathbf{u}_j)^2}{\left[ \sum_{j=1}^{2N} \mathbf{u}_j \cdot \mathbf{u}_j \right]^2}. \quad (3.1)$$

Here,  $\mathbf{u}_j$  is the displacement of atom  $j$  for the mode under consideration. For extended modes  $p^{-1}$  is of the order of  $1/N$ , and for modes strongly localized at a single site  $p^{-1} \sim 1$ . For a single Si atom placed in a pure Ge host, we find  $p^{-1} \approx 0.85$ , and placed in an  $x = 0.75$  virtual crystal  $p^{-1} \approx 0.79$ . This indicates that these single Si atom cluster modes are strongly localized and we expect larger clusters to be localized to a similar degree.

In Fig. 3 the computed Raman spectra of  $c\text{-Si}_{1-x}\text{Ge}_x$  are presented for three choices of the composition ratio and for two (parallel and crossed) scattering configurations. The position and width of the extended Ge-Ge mode at  $\omega \approx 30 \text{ cm}^{-1}$  were calculated using the CPA [added to the width was the anharmonic decay width of FWHM value  $0.99 \text{ cm}^{-1}$  (Ref. 30)], and the positions and amplitudes of the other modes computed using the mass-defect Green's-function approach described above, with a Lorentzian broadening of  $10 \text{ cm}^{-1}$  FWHM included for each mode. The calculations were performed with the choice of laser energy of  $\hbar\omega_L = 2.41 \text{ eV}$  and at temperature  $T = 293 \text{ K}$  to facilitate comparison with the observed spectra presented in Fig. 1 of Ref. 14 (the experimental spectrum for  $x = 0.77$  is reproduced in Fig. 3). The samples measured in Ref. 14 were grown by means of liquid-phase epitaxy (LPE) and are thus expected to have a random distribution of Si and Ge atoms. The relative weakness of the calculated  $x = 0.99$  spectra is probably due to the laser energy becoming resonant with the  $E_1$  transition at  $x \approx 0.83$  in the virtual-crystal band structure, thus strengthening the  $x = 0.90$  and  $0.75$  spectra.

The emphasis of this study is the local modes most

clearly visible in the  $x = 0.75$  spectra of Fig. 3, labeled  $2_1$  to  $5_1$  and Si-Ge. The notation  $N_M$  refers to a mode arising from a cluster of  $N$  Si atoms, with  $M$  being a convenient index for labeling increasingly energetic modes. The Si-Ge peak is due to isolated Si atoms with Ge nearest neighbors. With decreasing probability are the 2 to 5 Si atom clusters  $2_1$  to  $5_1$ . Although in many cases several different modes contribute to a single peak among  $2_1$  to  $5_1$ , generally there is a dominant mode and these are shown schematically in Fig. 4 for each of the labeled peaks in Fig. 3. As expected for Raman activity, the strongest peaks in Fig. 3 are due to the most symmetric TO-like vibrations since we see that all the modes in Fig. 4 have strong TO character. The less symmetric and the symmetric but acousticlike modes are also input into the Raman susceptibility calculation but do not contribute significantly to the calculated spectra. Shown in Fig. 5 is the phonon spectral function for  $\text{Si}_{0.01}\text{Ge}_{0.99}$ , displaying features for all modes, not just the Raman-active ones. It displays a multitude of acousticlike modes below the main peak at approximately  $380\text{ cm}^{-1}$ , and opticlike modes above. Many of the clusters have a mode with frequency close to that of an isolated Si atom; these contrib-

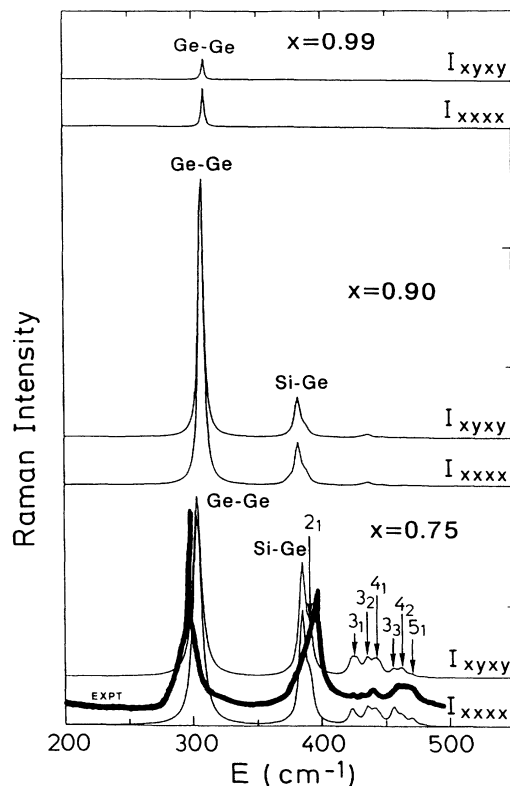


FIG. 3. Calculated Raman spectra for three choices of the alloy composition ratio, and for parallel ( $I_{xxxx}$ ) and crossed ( $I_{xyxy}$ ) scattering configurations. The crystal axes are defined as  $\hat{x} \parallel [110]$ ,  $\hat{y} \parallel [112]$ , and  $\hat{z} \parallel [111]$ . The vertical scale is in arbitrary units, but is the same for all composition ratios. Eigendisplacements for the labeled modes are given in Fig. 4. The thick line marked "EXPT" is the observed unpolarized spectrum for  $x = 0.77$  obtained from Ref. 14; it is scaled to give a Si-Ge peak of the same amplitude as in the  $I_{xxxx}$ ,  $x = 0.75$  calculated spectrum.

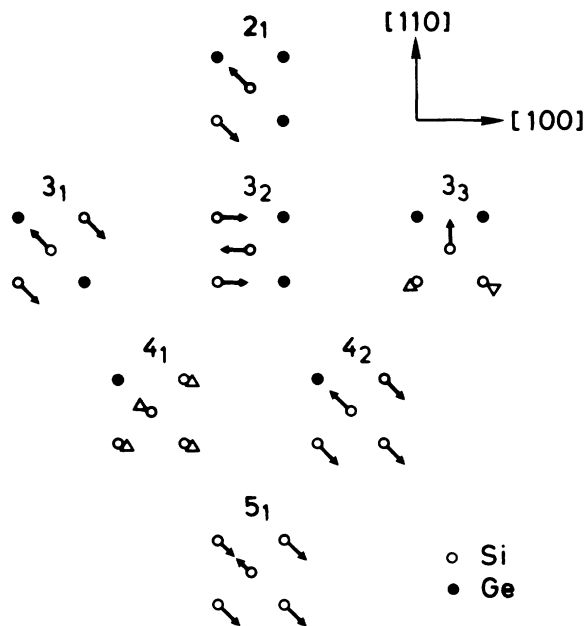


FIG. 4. Eigendisplacements of the local vibrational modes labeled in the  $x = 0.75$  spectra of Fig. 3. All atomic positions are projected onto the (001) plane. The atom in the lower-left-hand corner of each cluster is located at  $-(a/8)(1,1,1)$ , where  $a$  is the lattice spacing, and the origin of the coordinate system is midway between this atom and the central atom of the cluster. The central atom is bonded with the corner atoms. Displacements in the (001) plane are indicated by arrows, and displacements with a component into or out of the plane are indicated by triangles.

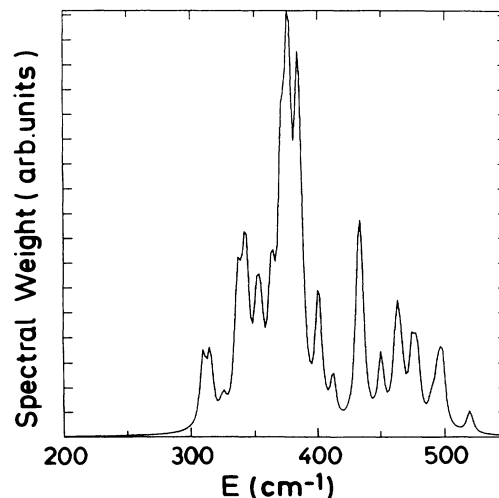


FIG. 5. Phonon spectral function for  $\text{Si}_{0.01}\text{Ge}_{0.99}$ . Each local mode for each cluster configuration (and the Ge-Ge extended mode) contributes with equal weight to the spectral function, thus this does not represent the phonon density of states. The spectral function shows the contributions of all calculated phonon modes and thus is considerably more detailed than the spectra of Fig. 3, where only Raman-active modes contribute.

ute to the significant strength of the main peak in Fig. 5. Of the seven calculated Raman peaks  $2_1$  to  $5_1$ , five ( $3_1$  to  $4_2$ ) are visible in the observed  $x=0.77$  spectrum of Ref. 14. The relative amplitudes do not always agree with experiment, possibly due to having compared calculated polarized spectra with measured unpolarized ones, but more probably because of the approximations involved in the calculations, such as considering clusters involving no more than five Si atoms (approximating larger clusters by a virtual-crystal host around smaller clusters) and possibly also due to neglecting the vibrations of the Ge atoms. The frequencies of the various peaks do, however, agree well with experiment, making our cluster assignments quite conclusive. Our calculations place the  $2_1$  mode at a slightly higher frequency than that of Si-Ge, whereas the experimental data suggest that the Si-Ge peak is broadened by it on the low-frequency side. A more detailed incorporation of force-constant changes and anharmonic effects may improve the agreement between the relative positions of the Si-Ge and  $2_1$  peaks. The weakest feature in our calculations,  $5_1$ , is not visible in the experimental data.

#### IV. SUMMARY

Cluster calculations have been performed to determine the frequencies and normal modes of local phonons in Ge-rich  $c\text{-Si}_{1-x}\text{Ge}_x$  alloys. We find that a mass-defect Green's-function approach and a microscopic calculation of the Raman susceptibility yield Raman spectra in excellent quantitative agreement with observations, leading to the identification of the various peaks in the fine structure with particular local vibrational modes. We estimate that this approach is valid for  $c\text{-Si}_{1-x}\text{Ge}_x$  with  $x \geq 0.75$ .

The calculations assume a completely random mixture of Si and Ge atoms, and describe well the experimental data for LPE-grown samples. Should the measured Raman spectra of other samples differ appreciably from those calculated here, this fact may be an indication of the presence of ordering in those samples.

#### ACKNOWLEDGMENT

C.G. acknowledges partial support of the Natural Sciences and Engineering Research Council of Canada.

\*Current address: Division of Applied Sciences, Harvard University, Cambridge, MA 02138.

<sup>1</sup>T. P. Pearsall, J. M. Vanderberg, R. Hull, and J. M. Bonar, *Phys. Rev. Lett.* **63**, 2104 (1989).

<sup>2</sup>R. Zachai, K. Eberl, G. Abstreiter, E. Kasper, and H. Kibbel, *Phys. Rev. Lett.* **64**, 1055 (1990).

<sup>3</sup>P. C. Kelires and J. Tersoff, *Phys. Rev. Lett.* **63**, 1164 (1989).

<sup>4</sup>F. K. LeGoues, V. P. Kesan, S. S. Iyer, J. Tersoff, and R. Tromp, *Phys. Rev. Lett.* **64**, 2038 (1990).

<sup>5</sup>F. K. LeGoues, V. P. Kesan, and S. S. Iyer, *Phys. Rev. Lett.* **64**, 40 (1990).

<sup>6</sup>S. de Gironcoli, P. Giannozzi, and S. Baroni, *Phys. Rev. Lett.* **66**, 2116 (1991).

<sup>7</sup>F. K. LeGoues, B. S. Myerson, and J. F. Morar, *Phys. Rev. Lett.* **66**, 2903 (1991).

<sup>8</sup>A. S. Barker, Jr. and A. J. Sievers, *Rev. Mod. Phys.* **47**, Suppl. 2, S1 (1975).

<sup>9</sup>D. W. Feldman, M. Ashkin, and J. H. Parker, Jr., *Phys. Rev. Lett.* **17**, 1209 (1966).

<sup>10</sup>A. E. Cosand and W. G. Spitzer, *J. Appl. Phys.* **42**, 5241 (1971).

<sup>11</sup>W. J. Brya, *Solid State Commun.* **12**, 253 (1973).

<sup>12</sup>S. C. Shen and M. Cardona, *Solid State Commun.* **36**, 327 (1980).

<sup>13</sup>M. A. Renucci, J. B. Renucci, and M. Cardona, in *Light Scattering in Solids*, edited by M. Balkanski (Flammarion, Paris, 1971), p. 326.

<sup>14</sup>M. I. Alonso and K. Winer, *Phys. Rev. B* **39**, 10 056 (1989); M. I. Alonso, Ph.D thesis, Universität Stuttgart, Germany, 1989.

<sup>15</sup>J. Humlíček, K. Navratil, M. G. Kekoua, and E. V. Khout-sishvili, *Solid State Commun.* **76**, 243 (1990).

<sup>16</sup>D. J. Lockwood, K. Rajan, E. W. Fenton, J. M. Baribeau, and M. W. Denhoff, *Solid State Commun.* **61**, 465 (1987).

<sup>17</sup>G. M. Zinger, I. P. Ipatova, and A. V. Subashiev, *Fiz. Tekh. Poluprovodn.* **11**, 656 (1977) [*Sov. Phys. Semicond.* **11**, 383 (1977)].

<sup>18</sup>Y. S. Chen, W. Shockely, and G. L. Pearson, *Phys. Rev.* **151**, 648 (1966); I. F. Chang and S. S. Mitra, *ibid.* **172**, 924 (1968).

<sup>19</sup>P. G. Dawber and R. J. Elliott, *Proc. Phys. Soc. London* **81**, 453 (1963).

<sup>20</sup>P. N. Keating, *Phys. Rev.* **145**, 637 (1966).

<sup>21</sup>I. M. Lifshitz, *Nuovo Cimento* **3**, 716 (1956).

<sup>22</sup>R. J. Elliott and P. Pfeuty, *J. Phys. Chem. Solids* **28**, 1789 (1967).

<sup>23</sup>W. Weber, *Phys. Rev. B* **15**, 4789 (1977); O. H. Nielson and W. Weber, *Comput. Phys. Commun.* **18**, 101 (1979).

<sup>24</sup>D. Strauch, A. P. Mayer, and B. Dorner, *Z. Phys. B* **78**, 405 (1990).

<sup>25</sup>C. H. Grein, S. Zollner, and M. Cardona, *Phys. Rev. B* **43**, 6633 (1991).

<sup>26</sup>D. Stroud and H. Ehrenreich, *Phys. Rev. B* **2**, 3197 (1970); S. Kline, F. H. Pollack, and M. Cardona, *Helv. Phys. Acta* **41**, 968 (1966); J. Humlíček, M. Garriga, M. I. Alonso, and M. Cardona, *J. Appl. Phys.* **65**, 2837 (1989).

<sup>27</sup>M. L. Cohen and T. K. Bergstresser, *Phys. Rev.* **141**, 789 (1960).

<sup>28</sup>M. Cardona and P. B. Allen, *Helv. Phys. Acta* **58**, 307 (1985).

<sup>29</sup>P. Soven, *Phys. Rev.* **156**, 809 (1967); D. W. Taylor, *ibid.* **156**, 1017 (1967).

<sup>30</sup>H. Fuchs, C. H. Grein, C. Thomsen, M. Cardona, W. L. Hansen, E. E. Haller, and K. Itoh, *Phys. Rev. B* **43**, 4835 (1991).

<sup>31</sup>H. Fuchs, C. H. Grein, M. I. Alonso, and M. Cardona, *Phys. Rev. B* **44**, 13 120 (1991).

<sup>32</sup>P. Dean, *Rev. Mod. Phys.* **44**, 127 (1972); R. J. Bell, *Rep. Prog. Phys.* **35**, 1315 (1972).